Applied Catalysis B: Environmental 219 (2017) 658–671

Contents lists available at ScienceDirect

Applied Catalysis B: Environmental

journal homepage: www.elsevier.com/locate/apcatb

Glycerol hydrodeoxygenation to 1,2-propanediol catalyzed by $CuPd/TiO_2$-Na

Alba N. Ardila[a,b,*], Marco A. Sánchez-Castillo[c], Trino A. Zepeda[d], Aída Luz Villa[e], Gustavo A. Fuentes[a]

[a] Research Group in Environmental Catalysis and Renewable Energies, Facultad de Ciencias Básicas Sociales y Humanas, Politécnico Colombiano Jaime Isaza Cadavid, Apartado Aéreo 49-32, Medellín, Colombia
[b] Department of Process Engineering, Universidad A. Metropolitana-Iztapalapa, San Rafael Atlixco 186, México, DF 09310, Mexico
[c] CIACYT, Universidad Autónoma de San Luis Potosí, Sierra Leona 550, San Luis Potosí, S.L.P., 78210, Mexico
[d] Nanoscience and Nanotechnology Center, Universidad Nacional A. de México, Ensenada, BC, 22800, Mexico
[e] Environmental Catalysis Research Group, CENIVAM, Universidad de Antioquia, SIU, Cra. 53 No. 61-30, Medellín, Colombia

ARTICLE INFO

Article history:
Received 15 January 2017
Received in revised form 17 July 2017
Accepted 1 August 2017
Available online 8 August 2017

Keywords:
Glycerol hydrodeoxygenation
1,2-Propanediol
Copper-palladium catalysts
Titania
Na effect

ABSTRACT

Copper-palladium bimetallic catalysts supported on TiO_2 were developed for the aqueous phase hydrodeoxygenation (HDO) of glycerol. Na-promoted bimetallic catalysts had higher activity than monometallic catalysts while maintaining high 1,2-propanediol (1,2-PDO) selectivity (76–93%) characteristic of Cu catalysts. The best results were obtained with $CuPd/TiO_2$-Na. At 220 °C and 0.7 MPa H_2 the initial turnover frequency (TOF based on Cu + Pd sites) was 0.14 s^{-1}; the selectivity to 1,2-PDO reached 85%. Characterization of the samples was performed by H_2-temperature programed reduction (H_2-TPR), X-ray diffraction and high-resolution electron microscopy (HRTEM) plus selected area electron diffraction (SAED), and their results were consistent with the formation of CuPd alloy nanoparticles with their surface enriched in Cu, hence explaining the high selectivity to 1,2-PDO of the bimetallics. The increased activity of the Pd-Cu bimetallic catalysts stems from the significantly smaller average diameter of the CuPd alloy nanoparticles when compared with the Cu or Pd nanoparticles of the monometallic catalysts. Besides the effect upon the nanoparticle structure, Pd promoted HDO in part by the activation of glycerol aqueous phase reforming to produce H_2 at the surface level. Cu was stabilized in the bimetallic samples by the formation of the alloy with Pd and by the presence of Na in the catalyst. As a result, $CuPd/TiO_2$-Na can be reused while maintaining high stable activity and 1,2-PDO selectivity. The HDO reaction proceeds through the formation of 1-hydroxy-2-propanone (acetol), followed by its hydrogenation to form 1,2 PDO. Formation of acetol or an acetol-like surface intermediate presumably occurs on support sites, whereas the hydrogenation to 1,2-PDO occurs on the metal sites. The first step is enhanced when basic sites are added to the support, while the hydrogenation step on Cu sites is improved by raising the H_2 pressure and/or by the formation of H_2 via reforming on Pd sites.

1. Introduction

The economic balance for biodiesel production is limited by the low price of glycerol, its main side-product; however, it is possible to add value by developing new glycerol-based catalytic processes, i.e., to produce industrially relevant chemicals such as acrolein, glyceric acid, lactic acid or propanediols (PDO) [1,2]. Among these compounds, 1,2-PDO is an important medium-value commodity chemical with annual production of roughly 1 million tons in the USA. It is used in the preparation of polyester resins, pharmaceuticals, cosmetics, fragrances and paints, among other products. It can also be used as a less toxic alternative to ethylene glycol-based deicing agents. The current industrial synthesis of 1,2-PDO involves hydrolysis of propylene oxide with water at temperatures between 125 and 200 °C and 2 MPa pressure [3,4].

There have been many efforts aimed at the conversion of glycerol to 1,2-PDO by catalytic HDO, one of the complex reaction pathways possible during hydrotreating of glycerol. This network can be envisioned as the competition between selective removal of one of the OH groups to form diols and then monoalcohols,

* Corresponding author at: Research Group in Environmental Catalysis and Renewable Energies, Facultad de Ciencias Básicas Sociales y Humanas, Politécnico Colombiano Jaime Isaza Cadavid. Apartado Aéreo 49-32, Medellín, Colombia.
E-mail addresses: anardila@elpoli.edu.co, albanellya@gmail.com (A.N. Ardila).

http://dx.doi.org/10.1016/j.apcatb.2017.08.006
0926-3373/

and the cleavage of C—C bonds leading to a mixture of lower alcohols, carboxylic acids, alkanes and also to full reforming to CO_2 and H_2. To favor HDO, a catalyst requires proper balance between hydro-dehydrogenation centers and a dehydration function. Cu-based catalysts have been found to achieve high selectivity for C—O bond hydro-dehydrogenation compared to C—C bond cleavage [2,5,6] but they are generally unstable. Pt, Ru, Au or Rh-containing materials are also active catalysts for this process [7,8], but their selectivity towards propanediols is not adequate because they promote excessive C—C cleavage. It is also possible to activate HDO by operating under basic conditions, especially when NaOH is added to the glycerol solution, although the literature indicates that C—C bond cleavage also increases, forming products such as ethylene glycol and methanol [9,10].

The poor stability of Cu-based catalysts for HDO results in rapid deactivation ascribed to sintering and/or leaching of the active species [11–13]. As an example, sintering of Cu particles in Cu/ZnO catalysts decreased the conversion of glycerol from 46 to 10% upon reuse [12]. A similar deactivation trend was observed with Cu/Al_2O_3 catalysts [13]. Only a few Cu-based catalysts have been demonstrated to be stable during glycerol HDO in aqueous media [14]. An approach to promote and stabilize Cu-based catalysts involves the addition of a small amount of noble metal (Pd, Rh, Re, Ru) [15–19], but the structural information of those catalysts is limited. An analysis of the information available shows that there is room for improvement, but detailed structural characterization of the active moieties and reaction pathways is still needed.

In order to design a better catalyst for the production of 1,2-PDO we chose to couple at the active site level Cu, a good glycerol hydrodeoxygenation catalyst, with Pd, a metal that exhibits moderate activity for aqueous phase reforming [20,21]. The idea is to facilitate the interaction of reaction intermediates with active hydrogen. We also were interested in its possible stabilizing effect upon metallic Cu. For a practical application in aqueous phase HDO or reforming of glycerol, the support was required to have good hydrothermal stability. Standard supports such as SiO_2, Al_2O_3, MgO, Nb_2O_5, and zeolites, among others, have stability issues leading to hydroxide formation and variations in surface area and porosity [22,23]. ZrO_2 and TiO_2 are more stable under reforming conditions [22,24], but we preferred TiO_2 because its anatase phase is stable in the temperature range of interest for HDO in contrast with the high-area tetragonal phase of ZrO_2.

In this paper, we report an improved catalyst, Cu-Pd/TiO_2 promoted by Na, for the valorization of glycerol by aqueous phase HDO into 1,2-PDO. It is highly active even under low H_2 pressure and addresses the drawbacks of Cu catalysts mentioned before. We determined the structure of the different nanoparticles formed on the surface of TiO_2 and analyzed the role of Pd and Na in improving or stabilizing the catalytic activity and selectivity of our materials.

2. Experimental

2.1. Catalyst synthesis

We synthesized mono- and bimetallic catalysts by wet-impregnation on TiO_2 (Degussa, P-25 powder). In all cases the loading of Pd or of Cu was set at 5 wt%. Pd/TiO_2 catalysts were prepared by impregnating the support with the required amount of $Pd(C_5H_7O_2)_2$ dissolved in acetone (5 mL acetone/g TiO_2). The resulting materials were oven-dried in air at 110 °C for 12 h, then heated to 400 °C at 2 °C/min, and held at that temperature for 2 h. Cu/TiO_2 catalysts were prepared similarly, but using an aqueous solution of $Cu(NO_3)_2{\cdot}3H_2O$ as the source of Cu (5 mL water/g TiO_2). Cu-Pd/TiO_2 catalysts (nominal atomic ratio Cu/Pd = 1.67) were prepared by sequential impregnation, starting with Cu; there were intermediate drying and calcination steps.

Table 1
Nomenclature used for Cu-Pd/TiO_2 catalysts.

Catalyst	Code
TiO_2	TiO_2
TiO_2-5%Na	TiO_2-Na
5%Cu/TiO_2	CuT
5%Cu/TiO_2-first reuse	CuT-R1
5%Cu/TiO_2-5%Na	CuT-Na
5%Pd/TiO_2	PdT
5%Pd/TiO_2-5%Na	PdT-Na
5%Cu-5%Pd/TiO_2	CuPdT
5%Cu-5%Pd/TiO_2-5%Na-Fresh	CuPdT-Na-F
5%Cu-5%Pd/TiO_2-5%Na-Washed	CuPdT-Na-W
5%Cu-5%Pd/TiO_2-5%Na-first reuse	CuPdT-Na-R1
5%Cu-5%Pd/TiO_2-5%Na-second reuse	CuPdT-Na-R2
5%Cu-5%Pd/TiO_2-5%Na-third reuse	CuPdT-Na-R3
5%Cu-5%Pd/TiO_2-5%Na-fourth reuse	CuPdT-Na-R4
5%Cu-5%Pd/TiO_2-0.5%Na	CuPdT-0.5Na
5%Cu-5%Pd/TiO_2-0.5%Na-first reuse	CuPdT-0.5Na-R1

The synthesis of Na-containing materials, either 0.5, 2.5 or 5 wt% Na, was done by first treating TiO_2 with NaOH dissolved in methanol (5 mL methanol/g TiO_2), followed by drying and calcination as mentioned above. Cu and/or Pd were then impregnated on Na-TiO_2 as done on TiO_2. Each of the materials was ground and sieved to diameters in the 74–105 μm range. Finally, just before its use in reaction, each sample was heated at 2 °C/min under flowing 10% H_2/Ar up to 300 °C, and held at that temperature for 3 h. Afterwards, the sample was cooled down to room temperature, still in H_2/Ar, and then quickly transferred to the reactor. The catalysts prepared in this study were coded as shown in Table 1.

2.2. Catalyst characterization

2.2.1. Quantitative analysis

Loading of Cu, Pd and Na in the fresh and used catalysts was verified by Atomic Absorption Spectroscopy (AAS) (Varian, model Spectra AA-20FS). In all cases the AAS value matched the nominal content within 5%.

2.2.2. Surface area

The surface areas of all catalysts were determined by the BET method from N_2 isotherms measured at 75.2 K with a Quantachrome Autosorb Automated instrument.

2.2.3. H_2-Temperature programmed reduction

H_2-Temperature programmed reduction (H_2-TPR) of the catalysts was carried out at 10 °C/min from 25 °C up to 800 °C, in the presence of 10% H_2/Ar (Infra, Mexico). The gas flow rate was 25 mL/min and it was kept constant using a mass flow controller. The apparatus was calibrated by reduction of 30 mg of CuO powder (99%, Merck) under the same experimental conditions.

2.2.4. X-Ray diffraction

The crystalline phases were determined from X-ray powder diffraction patterns collected in air at room temperature with a Bruker D-8 Advance diffractometer (Bragg-Brentano θ-θ geometry, Cu Kα radiation, a Ni 0.5% Cu-Kβ filter in the secondary beam, and a one-dimensional position-sensitive silicon strip detector (Bruker, Lynxeye)). The diffraction intensity was measured in the 15–80° 2θ range using a 0.02°/min 2θ step rate. The identification of the phases was made with the help of the Joint Committee on Powder Diffraction Standards files (JCPDS), and the data was processed using Jade 6.0 software.

2.2.5. Metallic dispersion

The metallic dispersion of our catalysts was calculated using chemisorption techniques specific to either Pd or Cu surface sites. They are described in the following sections.

2.2.5.1. Pd dispersion. The dispersion of Pd on mono- and bimetallic catalysts was determined by volumetric CO chemisorption (Micromeritics AutoChem 2920). We used a $metal_{surfacesite}$: CO_{ads} stoichiometry factor of 1, based on the work of Renouprez et al. [25] for Cu-Pd alloy particles. We verified that CO adsorption was specific to Pd surface sites by measuring adsorption on CuT and CuT-Na samples. CO adsorption was practically nonexistent, in agreement with the literature [26,27].

2.2.5.2. Cu dispersion. Nitrous oxide can be used for the estimation of the surface area of metallic Cu in catalysts, since N_2O oxidizes selectively the surface atoms of Cu crystallites between 20 and 120 °C. Thus, the Cu dispersion in the mono- and bimetallic catalysts was determined by sequential H_2 TPR – oxidation with N_2O – H_2 TPR [15,28]. Catalysts were first reduced in a 5% H_2/N_2, 10 °C/min at a flow rate of 30 mL/min while heating from room temperature to 450 °C. After the reactor was purged with He while cooling to 50 °C, 20% N_2O/N_2 (30 mL/min; 0.5 h) was used to oxidize surface Cu atoms to Cu_2O. Afterwards, the reactor was flushed with He to remove the oxidant and a second TPR experiment was performed. H_2 consumption in the second TPR was assigned to the reduction of surface Cu. The reactions involved were:

$$H_2 + CuO \rightarrow Cu^0 + H_2O$$

$$N_2O + 2\,Cu^0{}_s \rightarrow Cu_2O_s + N_2$$

$$H_2 + Cu_2O_s \rightarrow 2\,Cu_s + H_2O$$

Although the adsorption and decomposition of N_2O on Pd (110) has been reported [29], we verified that N_2O adsorption-decomposition on Pd-T and PdT-Na was negligible under our experimental conditions.

2.2.6. High resolution transmission electron microscopy and selected-area electron diffraction

Mono- and bimetallic catalysts were also analyzed by high-resolution transmission electron microscopy (HRTEM) in a JEOL 2100F electron microscope operated at 200 kV with a 0.19 nm resolution. Catalyst samples were deposited on a gold grid previously covered with a thin layer of carbon. To obtain the particle size distribution in each material we measured more than 100 particles from images taken from different areas and from different TEM specimens (all prepared by the same method). Diffraction patterns from the Cu-Pd bimetallic nanoparticles were obtained by selected-area electron diffraction (SAED). These patterns were calibrated against those of polycrystalline Au with known d-spacing that were collected under the same experimental conditions. This technique allowed us to determine the presence of a CuPd alloy.

2.3. Catalytic activity

Catalytic tests were carried out in a batch reactor (Parr Instruments). The reactor was loaded with 50 mL of a 20 wt% aqueous solution of glycerol and 0.3 g of the previously reduced catalyst. After it was sealed, the reactor was flushed with flowing N_2 at 0.1 MPa for 5 min to remove air from the headspace. N_2 was subsequently flushed with flowing H_2 at 0.1 MPa for 5 min. The reactor was then pressurized to 0.7 MPa with H_2 and heated under moderate agitation (100 rpm) to a final reaction temperature of 220 °C. Once this temperature was reached, an initial liquid sample was drawn to mark the start of the reaction and the rate of agitation was increased to 480 rpm. The reaction was allowed to proceed for 6 h while the liquid phase was sampled each hour. To determine the activity of the physical mixture of the monometallic catalysts, we loaded 0.3 g each of the solids containing 2.5 wt% Na, in order to have the same amount of Cu, Pd and Na in the reaction media throughout the tests.

The liquid reaction samples were analyzed by gas chromatography (Agilent 6850 GC equipped with a flame ionization detector (FID) and a HP-INNOWAX capillary column). The reaction products were also identified by GC–MS (Agilent 5975 GC–MS with a HP-PLOT Q column). Once the reactor was cooled to room temperature we collected gas samples from the headspace in gas sampling bulbs and analyzed them using two gas chromatographs equipped with thermal conductivity detectors (TCD): a Shimadzu GC-12A equipped with a Porapak Q packed column was used for detecting H_2 and a HP 5890 GC equipped with a HP-Plot Q capillary column detected light hydrocarbons, CO and CO_2.

The carbon balance in each experiment was determined from both liquid and gas phase compositions at the end of the reaction (6 h). It was always >93%. The missing carbon can probably be accounted for by losses during sampling of the reaction mixture. Glycerol conversion and product selectivities (carbon-based) were calculated on a molar basis using standard formulas. We estimated the catalytic activity for mono- and bimetallic catalysts using the initial turnover frequency (TOF) as given by Eq. (1).

$$\mathrm{TOF}\left(s^{-1}\right) = \frac{\text{Initial rate of glycerol consumed}(\text{mmol } s^{-1} g_{cat}{}^{-1})}{\text{Surface Cu or CuPd sites}\left(\text{mmol} g_{cat}{}^{-1}\right)} \quad (1)$$

In the case of the catalytic reactions over Na-promoted and unpromoted catalysts without external addition of hydrogen, the glycerol consumption and hydrogen production were determined only at the end of the reaction (6 h). The catalytic activity for these materials was estimated by calculating the turnover number (TON) as given by Eq. (2).

$$\mathrm{TON} = \frac{\text{Glycerol consumed } (\text{mmol} g_{cat}{}^{-1})}{\text{Surface Cu and/or Pd sites}\left(\text{mmol} g_{cat}{}^{-1}\right)} \quad (2)$$

3. Results and discussion

3.1. Surface and bulk characterization of catalysts

3.1.1. N_2 adsorption

The BET surface area (SA) of the solids was somewhat lower than that of TiO_2 as a result of the impregnation with Na, Pd, and/or Cu, presumably because of pore clogging. The SA was in the 43–59 m^2/g-cat range. A list of the different textural properties for all materials tested may be found in the Supplementary Information (Table S1).

3.1.2. X-Ray diffraction

Fig. 1 shows the XRD patterns of our materials. Peaks marked as A and R correspond to the anatase and rutile phases of TiO_2, respectively. Addition of Na did not modify significantly the crystalline structure of the support. In the case of the PdT catalyst there were two extra peaks centered at $2\theta = 40.2°$ and 46.7°, that correspond to the (111) and (200) planes of metallic Pd crystals. The same XRD reflections, with a slightly lower intensity, were observed with the PdT-Na catalyst, although broadened, particularly the (111) signal, an indication of increased Pd dispersion. In the case of Cu catalysts, the XRD pattern of CuT showed a weak reflection at $2\theta = 43.2°$ assigned to metallic Cu (111). The same reflection was present with CuT-Na, but there were two additional reflections at $2\theta = 35.4°$ and $2\theta = 50.4°$, attributed to the (002) and (200) planes

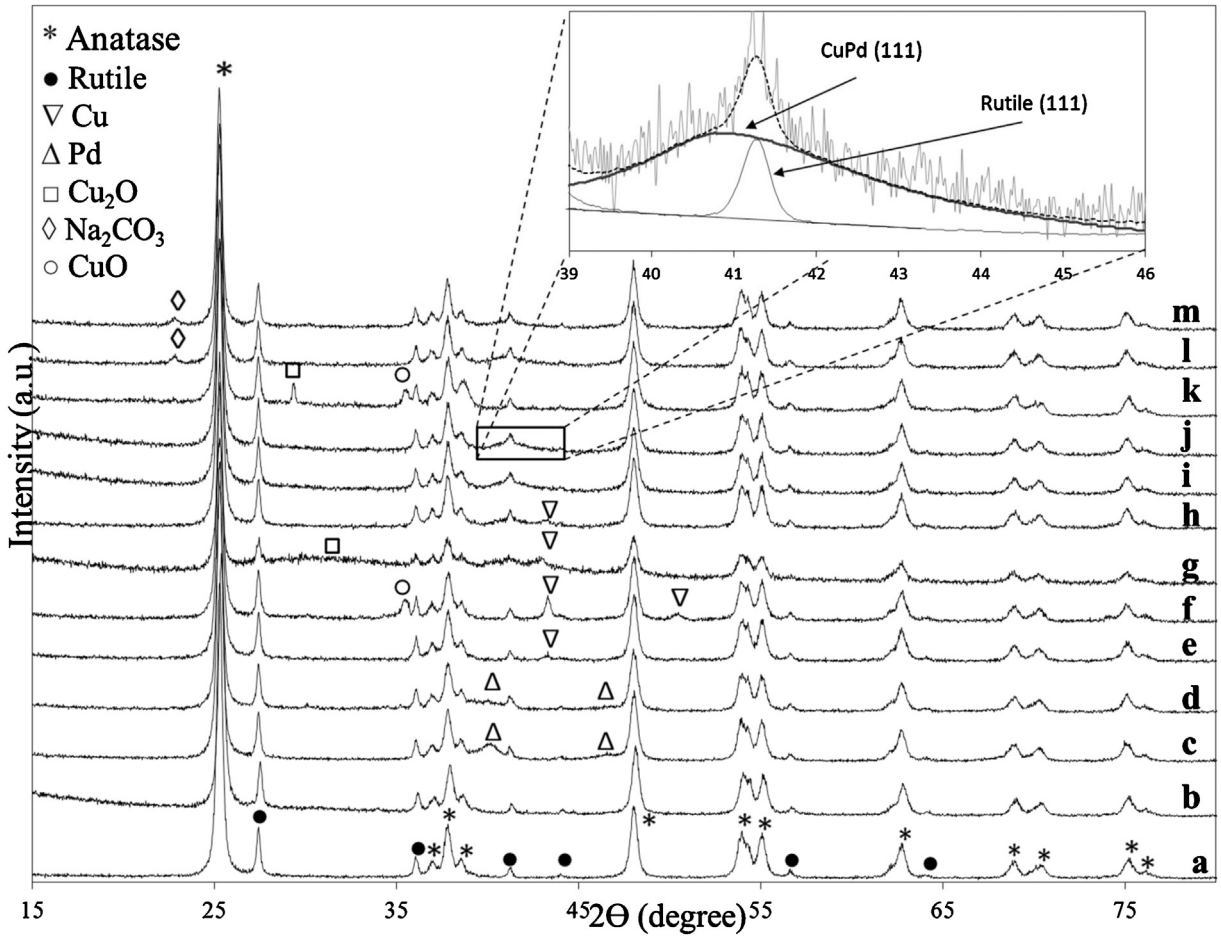

Fig. 1. XRD patterns of (a) TiO_2; (b) TiO_2-Na; (c) PdT; (d) PdT-Na; (e) CuT; (f) CuT-Na; (g) CuPdT; (h) CuPdT-0.5Na; (i) CuPdT-Na-W; (j) CuPdT-Na-F; (k) CuT-R1; (l) CuPdT-0.5Na; (m) CuPdT-Na-R3.

of CuO and metallic Cu, respectively, suggesting that the presence of Na restricted partially the reduction of CuO to Cu^0, in agreement with the literature [30,31]. The (111) reflection for Cu in the CuT-Na catalyst was narrower than that observed in CuT, i.e., the Cu crystallites were larger when Na was present in the support.

XRD patterns of the CuPdT and CuPdT-0.5Na catalysts reveal the presence of partially reduced Cu (Cu_2O (110), $2\theta = 30.5^\circ$) and of reduced Cu (Cu (111), $2\theta = 43.2^\circ$). A close analysis of the XRD patterns for the CuPdT-Na-F and CuPdT-Na-W bimetallic catalysts (see the inset plot in Figs. 1 and S1–S2 in the Supplementary Information) evidences the presence of a broad peak centered at $2\theta = 40.8^\circ$, overlapped with the diffraction peak of rutile (111). It corresponds to the (111) reflection of CuPd, i.e., an alloy, present as small nanoparticles. The formation of a CuPd alloy has been detected on other Cu-Pd systems using EXAFS [32,33], XPS and XRD [32,34,35]. Interestingly, the XRD pattern from CuPdT-Na reused catalysts did not show peaks corresponding to partially reduced or metallic Cu. In this case a new peak appeared at $2\theta = 22.8^\circ$, assigned to a small amount of Na_2CO_3 (PCPDF #19-1130) formed during reaction on the surface of the catalysts.

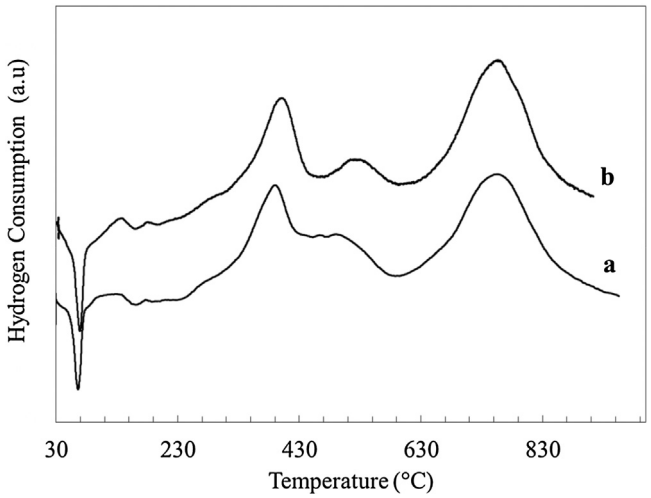

Fig. 2. H_2-TPR profile of (a) PdT; (b) PdT-Na.

3.1.3. H_2-TPR

H_2-TPR was sensitive to the composition of our materials and to the interaction between Cu and Pd in the bimetallic samples. Besides the features characteristic of the supported metal reduction, all our materials had also a broad H_2-TPR band in the 717–783 °C range that corresponds to the reduction of TiO_2 [36,37]. The maximum of that band decreased about 30 °C when the Na content increased from 0 to 5 wt%, an effect that has been observed in samples consisting of noble metals supported on TiO_2 and that has been assigned to the formation of new sites in the metal-support interface [38,39].

H_2-TPR profiles of the monometallic PdT and PdT-Na catalysts are shown in Fig. 2. They exhibit a desorption peak with minimum at about 66–72 °C, assigned to the decomposition of β-PdH (Pd hydride; reported to decompose in the 50–100 °C range [40]), pre-

Table 2
H_2/metal molar ratio from TPR experiments.

Sample	Peak maximum, °C	H_2/Metal, mole/mole
PdT	66	0.95
	380, 488	
	747	
PdT-Na	72	0.99
	394, 516	
	750	
CuT	493	0.75
	717	
CuT-Na	456	0.81
	735	
CuPdT	56	1.02
	115	
	783	
CuPdT-0.5Na	72	1.03
	131	
	771	
CuPdT-Na-F	90	1.09
	164	
	750	
CuPdT-Na-W	80	1.07
	158	
	760	

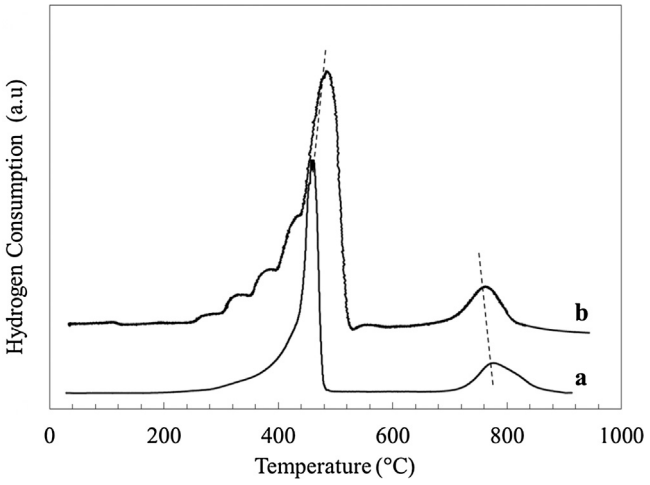

Fig. 3. H_2-TPR profile of (a) CuT; (b) CuT-Na.

sumably formed by reduction of small-sized PdOx moieties when exposed to H_2 at room temperature. A broad asymmetric reduction peak is observed at higher temperatures, with a maximum at 380 °C for PdT and at 394 °C for PdT-Na, and shoulders at about 488 °C in the first case and at 510 °C when Na was present. Such TPR patterns for Pd catalysts are observed when high temperature calcination is used [41], and they have been assigned to the reduction of PdO species interacting strongly with supports such as TiO_2 and Al_2O_3 [42,43]. The structure of the surface PdOx moieties has not been elucidated; they have been considered to form a 2-dimensional surface complex in the case of Pd/Al_2O_3, or referred to as [PdO]SC to imply a support-component strong interaction [42]. The integrated H_2/Pd molar ratio for these catalysts, reported in Table 2, is close to 1, the stoichiometric value for the PdO → Pd reduction.

The H_2-TPR results for CuT and CuT-Na monometallic catalysts are shown in Fig. 3. CuT has a single broad reduction peak with maximum at about 456 °C. In the case of CuT-Na the maximum shifts 37 °C upwards and several shoulders appear on the low temperature branch of the reduction trace, a characteristic assigned to the reduction of highly dispersed CuO species [32,44]. The H_2/Cu molar ratios during the reduction of CuT (0.75) and of CuT-Na (0.81)

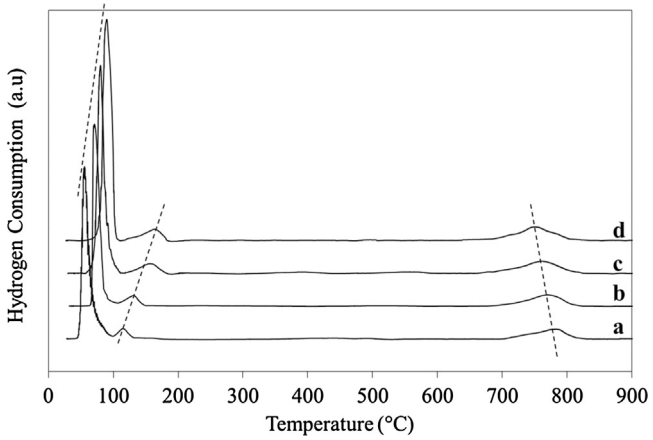

Fig. 4. H_2-TPR profile of (a) CuPdT; (b) CuPdT-0.5Na; (c) CuPdT-Na-W; (d) CuPdT-Na-F.

Table 3
Pd and Cu dispersion of mono- and bimetallic catalysts.

Catalyst	Pd dispersion (%)	Cu dispersion (%)
PdT	25	–
PdT-Na	29	–
CuT	–	16
CuT-R1	–	11
CuT-Na	–	7
CuPdT	4	26
CuPdT-Na-F	6	17
CuPdT-Na-R1	9	21
CuPdT-Na-W	9	19
CuPdT-0.5Na	7	22
CuPdT-0.5Na-R1	7	25

are below 1, presumably because there is partial reduction of Cu^{2+} during calcination.

The reduction pattern for the bimetallic Cu-Pd bimetallics was very different from those of the monometallics, an evidence of the Cu-Pd interaction on the surface of TiO_2. All Cu-Pd bimetallic samples reduced at much lower temperatures than either one of the monometallics (Fig. 4), experiencing a sharp reduction process with a maximum between 56 and 90 °C, followed by a second broad process with maximum in the 115–164 °C range. An upward shift in temperature occurred when Na was present in the support. In all cases the H_2/(Cu + Pd) molar ratio was close to 1, indicating complete metallic reduction. There was no evidence for the formation of β-PdH, but if small amounts of the hydride were formed and decomposed, that signal would be masked by the large reduction trace present below 100 °C.

The shift of the TPR trace to low temperatures when Cu and Pd are combined on the bimetallic materials is another evidence for the formation of a CuPd alloy, in agreement with our XRD analysis. The shift to low temperature reduction might be activated initially by the reduction of Pd present in small ensembles of a mixed Cu + Pd oxide. H_2 activation on the Pd nuclei would facilitate the reduction of Cu and of larger sized oxidic ensembles, leading to the formation of bimetallic nanoparticles. Our observations agree with recent reports by Xia et al. [15] and Molenbroek et al. [45].

3.1.4. Pd and Cu dispersion

Pd and Cu dispersions for mono- and bimetallic catalysts are summarized in Table 3. The small variation in the dispersion of the monometallics when the support was modified with Na agrees with the literature [30,36,46]. In the case of the bimetallic catalysts, both Cu and Pd dispersions varied significantly when compared with the corresponding monometallic dispersions. The Cu dispersion was

Table 4
Average particle size determined by XRD and TEM for mono- and bimetallic catalysts.

Catalyst	d_{TEM-S} (nm)	d_{TEM-V} (nm)	d_{XRD} (nm)
PdT	5.5	6.6	Pd (111) = 6.9 Pd (200) = 6.0
PdT-Na	3.8	4.5	Pd (111) = 2.5 Pd (200) = 4.8
CuT	9.5	14.0	Cu (111) = 15.2
CuT-Na	21.7	23.3	Cu (111) = 24.1 Cu (200) = 15.9 CuO (002) = 19.5
CuT-R1	11.8	15.5	Cu_2O (110) = 41.0 CuO (002) = 23.0
CuPdT	3.4	3.7	Cu_2O (110) = 9.0 CuPd (111) = 2.9
CuPdT-Na-F	3.9	5.5	CuPd (111) = 3.7
CuPdT-Na-W	5.7	5.7	CuPd (111) = 4.0
CuPdT-Na-R3	4.6	5.0	CuPd (111) = 3.6
CuPdT-0.5Na	5.1	5.3	CuPd (111) = 3.8
CuPdT-0.5Na-R1	5.3	5.8	CuPd (111) = 3.5

larger, and that of Pd lower. The enhancement in Cu dispersion when combined with Pd has been reported in the literature [15–17], but there are no references to the dispersion of Pd. The global exposure of surface sites of each of the metals present in a bimetallic is affected in part by the particle size distribution –the classical explanation when only monometallics are involved- plus the possibility of having variations in surface composition when a solid mixture, i.e. an alloy, is formed. We have evidence from XRD and H_2-TPR that CuPd alloy nanoparticles are present on Cu-Pd/TiO_2 with and without Na, and our chemisorption results suggest that the surface of these nanoparticles is enriched with Cu, in agreement with the reported segregation of Cu to the surface of a CuPd alloy [45,47–49]. The surface composition based on chemisorption alone gives a Cu/Pd ratio of about 2.65, well above the value expected for a homogeneous alloy based on the Cu/Pd molar ratio of the sample (1.67). Our XRD measurements also indicate that there are differences in crystallite mean diameter when comparing mono- and bimetallic catalysts. This is further discussed in the next section on HRTEM measurements.

3.1.5. The structure of the CuPd nanoparticles using TEM, HRTEM and SAED

We determined the size and the structure of the nanoparticles in our catalysts using TEM and HRTEM analysis. The TEM micrographs of all tested catalysts are shown in Fig. 5, together with their nanoparticle size distribution histograms. We also determined the average nanoparticle size of our catalysts either by TEM or by XRD line broadening using the Scherrer formula. Given that the last technique estimates the volume-weighted average diameter of the crystallites, a corresponding mean nanoparticle was calculated from our TEM data: $d_{TEM-V} = \Sigma n_i d_i^4 / \Sigma n_i d_i^3$, see [49]. The average nanoparticle diameters for our samples are given in Table 4. In the case of the bimetallic catalysts, the crystallite sizes determined by XRD are systematically smaller than those obtained by TEM. There is indication in the literature that extra XRD broadening may occur if there is a gradient of composition in alloy nanoparticles [49], hence resulting in an underestimation of their mean particle size in that case.

The average particle size of the CuT catalyst (9.5 nm) is smaller than that obtained for CuT-Na (22 nm), in agreement with the dispersion values already reported in Table 3. The effect of Na upon the Pd nanoparticles is the opposite, i.e. there is an increase in the Pd dispersion when Na is present in TiO_2. The average nanoparticle size in the bimetallic samples is the smallest, it is in the 5.0–5.7 nm range, regardless of Na content. The small nanoparticle diameter results in an increased exposure of metallic surface sites and in an increase in the overall reactivity of these catalysts, reported in the next section.

Table 5
Indexing data of crystal faces from the inner to the outer ring for bimetallic particles.

Ring	Crystal plane distance (Å)	Miller Index (*hkl*)
(a) CuPdT		
R1	2.18	(1 1 1)
R2	1.87	(2 0 0)
R3	1.34	(2 2 0)
R4	1.14	(3 1 1)
(b) CuPdT-Na-F		
R1	2.17	(1 1 1)
R2	1.88	(2 0 0)
R3	1.33	(2 2 0)
R4	1.13	(3 1 1)
(c) CuPdT-Na-F		
R1	2.19	(1 1 1)
R2	1.87	(2 0 0)
R3	1.35	(2 2 0)
R4	1.12	(3 1 1)
(d) CuPdT-Na-R3		
R1	2.18	(1 1 1)
R2	1.88	(2 0 0)
R3	1.34	(2 2 0)
R4	1.13	(3 1 1)

To analyze the detailed structure of our best catalysts, the bimetallics, we performed HRTEM and SAED measurements of CuPdT, CuPdT-Na-F and CuPdT-Na-R3. Figs. 6–8 include representative HRTEM images of CuPdT, CuPdT-Na-F and CuPdT-Na-R3 catalysts. The bimetallic nanoparticles in all catalysts have well-developed crystalline structures with continuous ordered lattice fringes. Based on a digital Fourier transform analysis of the lattice spacing from different areas of the nanoparticles, we determined that the interplanar spacings in the CuPdT catalyst measured 0.218 nm, 0.186 nm and 0.136 nm, and correspond to the (111), (200) and (220) interplanar distances of the cubic CuPd alloy (ICDD card No. 48-1551). In the case of the CuPdT-Na-F sample, we determined that the lattice spacing across three interplanar spacings were 0.186 nm, 0.134 nm and 0.113 nm, which correspond to the (200), (220) and (311) crystal planes of the same cubic CuPd alloy. Interestingly, a close examination of the micrographs revealed the presence of NaOx and of Na_2CO_3, the latter in catalysts already used in reaction. Multilayers of NaOx on both TiO_2 and CuPd are readily observed on CuPdT-Na-F (Fig. 7) and CuPdT-Na-R3 (Fig. 8). They have poorly resolved lattice fringes, a feature characteristic of mixed species.

The SAED patterns of the bimetallic particles, shown in Fig. 9, consist of polycrystalline diffraction rings. From the inner to the outer rings they were indexed as the (111), (200), (220) and (311) crystal faces of CuPd (see Table 5). This technique also shows that the alloyed CuPd particles have cubic symmetry. SAED values are in excellent agreement with those calculated from HRTEM and XRD, and further confirm the existence of CuPd alloy nanoparticles on the surface of TiO_2.

The combined characterization results in this work indicate that our bimetallic catalysts, Cu-Pd/TiO_2 and Cu-Pd/TiO_2-Na, consist primarily of supported CuPd alloy nanoparticles with an average diameter of 4 nm, smaller than the diameters of Cu or Pd nanoparticles in the monometallic samples. The CuPd nanoparticles form at temperatures well below those needed to fully reduce Cu or Pd in samples pretreated at high temperatures. Cu is stabilized in the alloy, and it enriches the surface of the nanoparticles. These structural features have not been reported previously in the literature. Their impact on the catalytic properties of our materials is discussed in the next section.

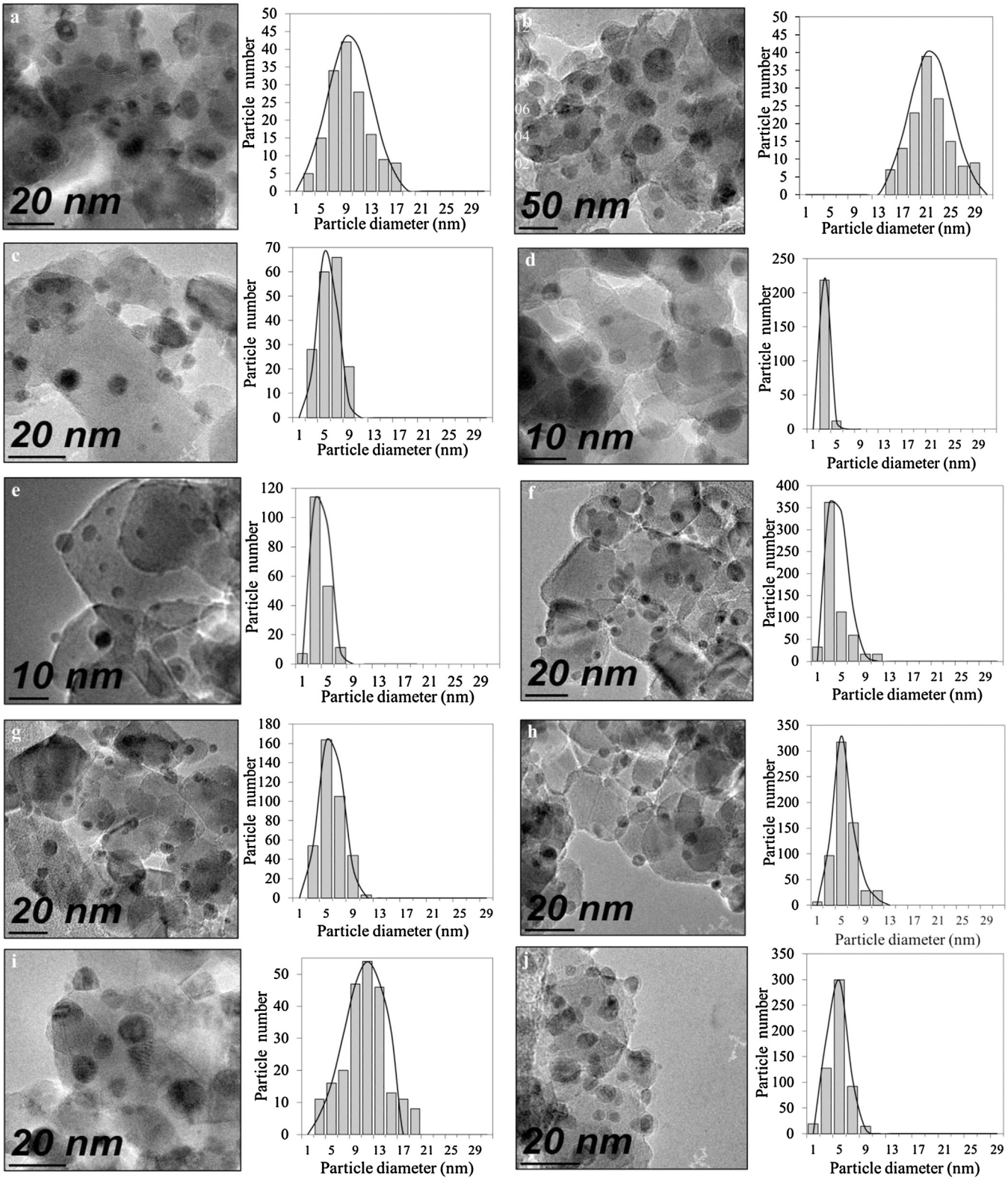

Fig. 5. TEM images: (a) CuT; (b) CuT-Na; (c) PdT; (d) PdT-Na; (e) CuPdT; (f) CuPdT-Na-F; (g) CuPdT-Na-W; (h) CuPdT-0.5Na; (i) CuT-R1; (j) CuPdT-Na-R3 and their corresponding nanoparticle size distribution histograms.

3.2. Catalytic performance

We performed a series of glycerol conversion experiments with and without H_2 in the headspace of the reactor in order to uncouple reactions and get information about the pathway from glycerol to 1,2-PDO, i.e. by turning off the hydrogenation step. Those experiments also helped us determine the occurrence of aqueous phase reforming and to study the effect of Cu-Pd alloying upon the overall catalytic activity and selectivity. The effect of adding basic sites through the incorporation of Na to TiO_2 was also analyzed.

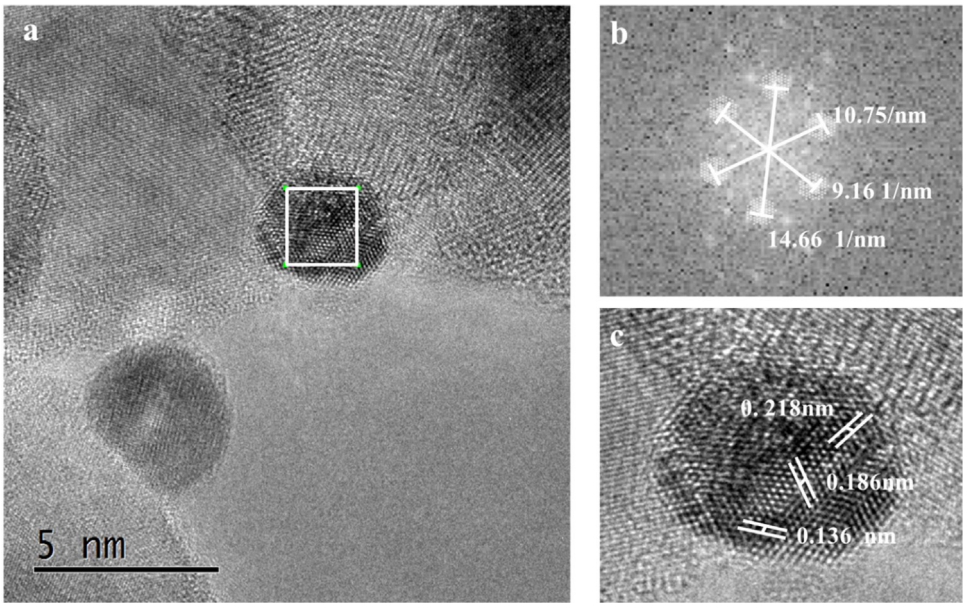

Fig. 6. (a) HRTEM image for CuPdT; (b) FFT from CuPd bimetallic particles; (c) Average inverse FFT for the interplanar spacing from the CuPd alloy.

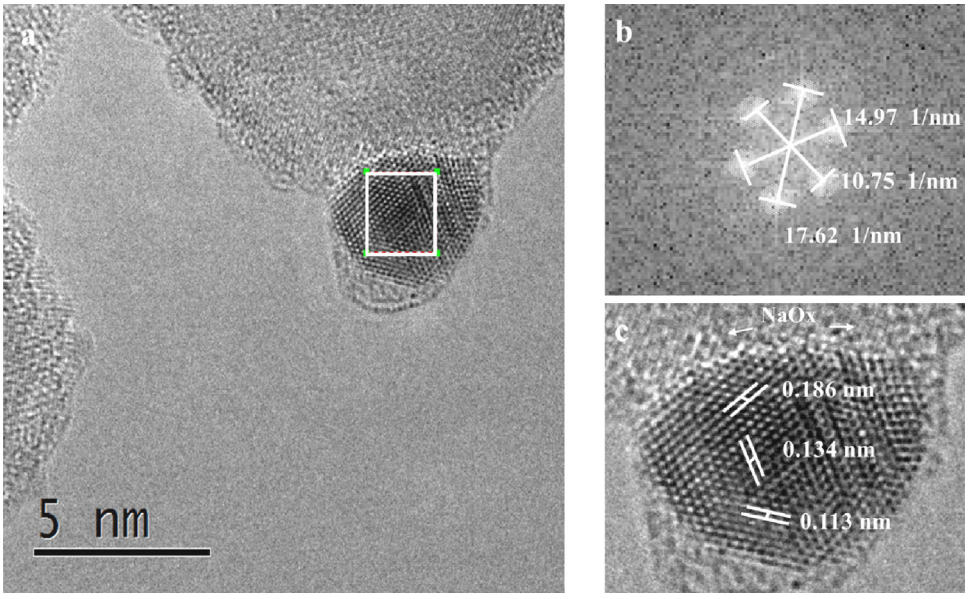

Fig. 7. (a) HRTEM image for CuPdT-Na-F; (b) FFT from CuPd bimetallic particles; (c) Average inverse FFT for the interplanar spacing from the CuPd alloy.

3.2.1. Glycerol conversion in the absence of H_2

The monometallic and bimetallic catalysts were tested for the conversion of glycerol in the absence of H_2 in the initial reaction mixture. The results are given in Table 6. The major products identified in the liquid phase were acetol and 1,2-PDO, with traces of *n*-propanol, ethanol, methanol, acetaldehyde, propionaldehyde, acetone, acetic acid and propionic acid. Gas phase products included H_2, CO_2 and CO, and were more important when Pd was present, an evidence for its higher reforming activity when compared to Cu. Monometallic Cu catalysts, although less active, had higher selectivity to acetol and 1,2-PDO. Cu-Pd bimetallic catalysts were the most active, and also favored the formation of acetol, followed by 1,2-PDO. The gas phase concentration of H_2 and CO_2 was smaller than with PdT or PdT-Na, presumably because the surface of the bimetallic nanoparticles was enriched with Cu, limiting the exposure to Pd sites active in reforming. The bimetallics were reused without losing activity, an indication of the stability of the CuPd nanoparticles present on these materials. In all cases the effect of Na was to increase reactivity, in agreement with the literature [7–10], presumably stemming from the formation of extra basic sites on the surface of TiO_2 that favor the dehydration of glycerol to acetol [38,39].

In this set of experiments, the conversion of acetol to 1,2-PDO was restricted by the limited availability of active hydrogen in the reaction medium. The residual hydrogenation observed stems from the H_2 generated through reforming. These observations are in line with the sequential nature of the mechanism of hydrodeoxygenation [50] that involves the dehydration on the support sites to form acetol or a precursor that is further hydrogenated to 1,2-PDO on the metallic sites.

The TON values reported in Table 6 can then be rationalized by referring to our characterization results. Monometallic Pd catalysts produced more H_2 and had higher glycerol TON, which measures both HDO and reforming. Cu and CuPd catalysts had large produc-

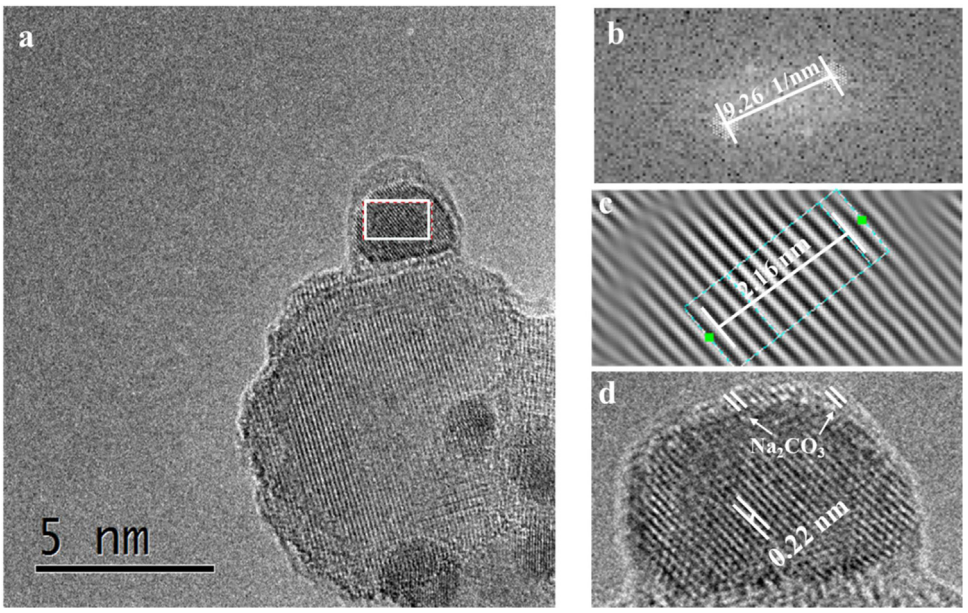

Fig. 8. (a) HRTEM image for CuPdT-Na-R3; (b) FFT from CuPd bimetallic particles; (c) Inverse FFT for selected region (10 interplanar spacings) from the CuPd alloy; (d) Average inverse FFT for the interplanar spacing from the CuPd alloy.

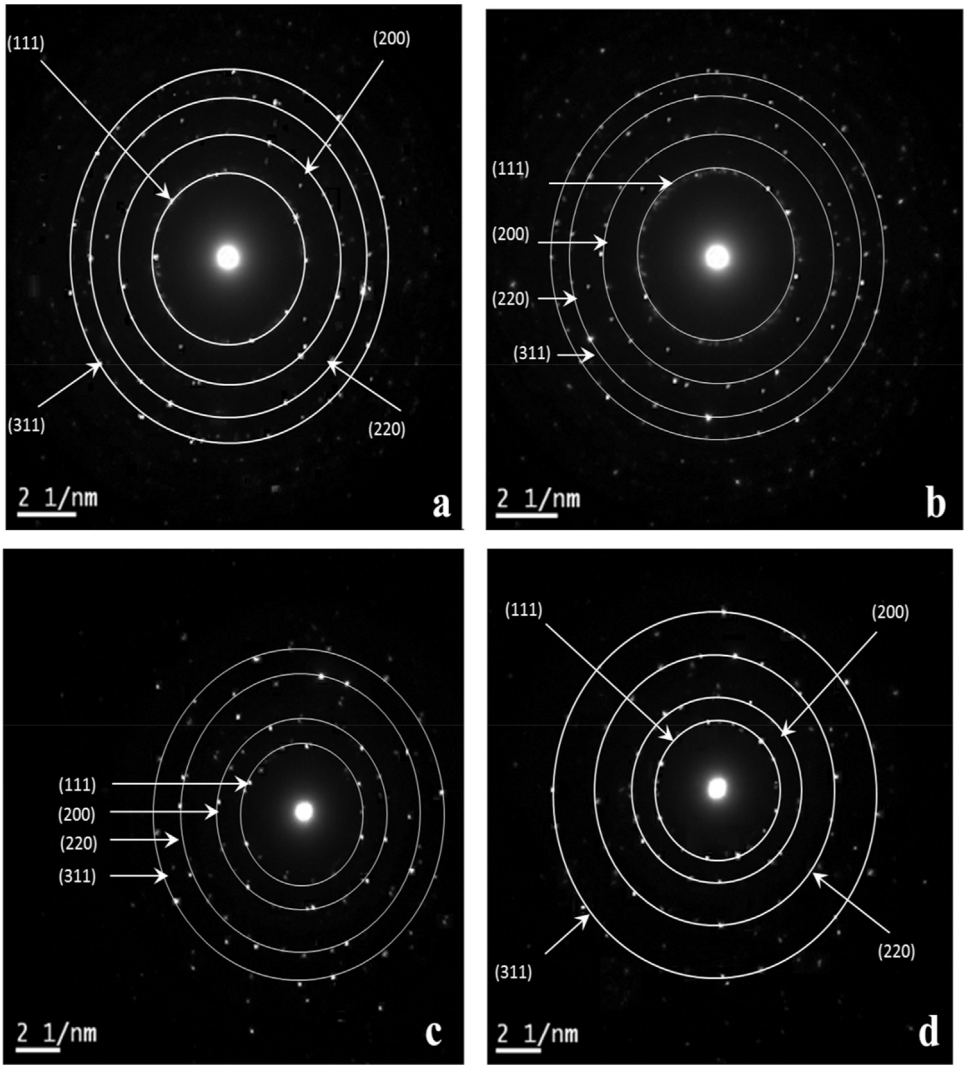

Fig. 9. SAED patterns showing polycrystalline diffraction rings acquired from some bimetallic particles. (a) CuPdT; (b) and (c) CuPdT-Na-F; (d) CuPdT-Na-R3.

Table 6
Glycerol conversion, carbon selectivity, glycerol TON, H_2 TON and carbon balance for Na-promoted and unpromoted catalysts in the absence of H_2.

Catalyst	Glycerol conversion (%)	Carbon selectivity (%)					TON $H_2/10^2$	TON Glycerol/10^2	Carbon balance (%)
		1,2-PDO	Acetol	CO_2	CO	Others*			
CuT	8.6	54.5	35.0	0.1	0	10.4	0.04	2.8	98
CuT-Na	11.6	42.8	52.4	0.2	0	4.6	0.12	7.8	94
PdT	18.4	34.1	19.1	19.2	0.3	27.3[a]	0.14	6.3	97
PdT-Na	28.7	29.7	25.5	39.6	2.1	3.1	1.04	8.2	93
CuPdT	25.6	30.1	54.3	1.7	0	13.9	0.23[b]	4.4[b]	96
CuPdT-Na-F	38.7	19.6	69.4	2.5	0.2	8.3	0.54[b]	9.0[b]	93
CuPdT-Na-W	34.1	22.0	67.0	1.6	0	9.4	0.18[b]	6.7[b]	97
CuPdT-Na-R1	33.0	25.1	59.4	2.0	0	13.5	0.17[b]	6.1[b]	98
CuPdT-0.5Na	34.0	24.0	62.6	2.1	0	11.3	0.16[b]	6.3[b]	97
CuPdT-0.5Na-R1	35.0	19.6	65.4	2.0	0	6.7	0.14[b]	6.0[b]	98

Reaction conditions: 20 wt% glycerol aqueous solution (50 mL), 0.7 MPa N_2 pressure, 0.3 g catalyst, 220 °C, 6 h. * Other products include minor amounts of alcohols (ethanol, methanol (selectivity <1%) and *n*-propanol), as well as traces of oxygenates such as acetaldehyde, propionaldehyde, acetone, ethylene glycol (selectivity <2%), acetic acid and propionic acid, which were identified by mass spectrometry. [a] For PdT catalyst the others include majorly ethylene glycol (selectivity ~20%). [b] TON based on surface Cu + Pd sites.

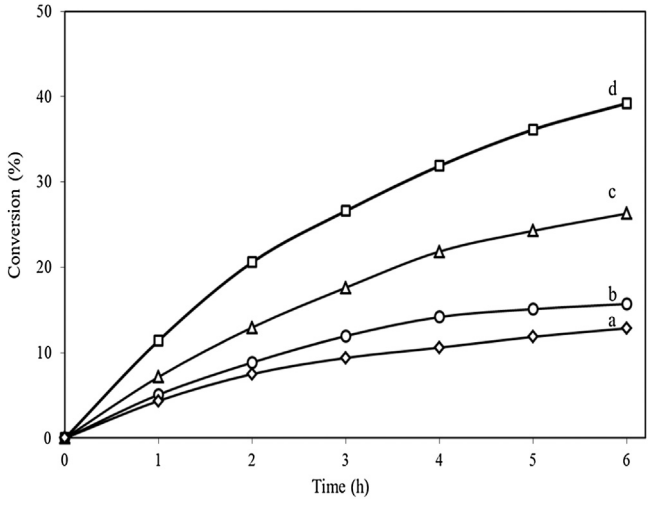

Fig. 10. Glycerol conversion as a function of time over (a) CuT; (b) PdT; (c) admixture of CuT and PdT; (d) CuPdT. Reaction conditions: 20 wt% glycerol aqueous solution (50 mL), 0.7 MPa H_2 pressure, 0.3 g catalyst, 220 °C, 480 rpm, 6 h.

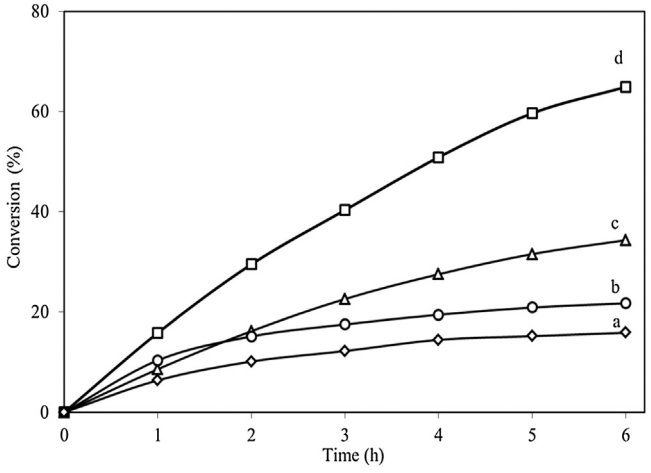

Fig. 11. Effect of Na presents on Cu-based catalysts during glycerol conversion: (a) CuT-Na; (b) PdT-Na; (c) admixture of CuT-Na and PdT-Na; (d) CuPdNa-F. Reaction conditions: 20 wt% glycerol aqueous solution (50 mL), 0.7 MPa H_2 pressure, 0.3 g catalyst, 220 °C, 480 rpm, 6 h.

tion of acetol because the hydrogenation step was limited by the low production of H_2 through reforming. CuPd catalysts had similarities with Cu catalysts because the surface of the nanoparticles is enriched with that metal, but the presence of Pd sites fostered reforming above the values for monometallic Cu. Our results are in line with literature reports about the high efficiency for C—O bond hydro-dehydrogenation and poor activity for C—C bond cleavage of Cu-based catalysts [5,6,12] and about the selectivity of Pd catalysts towards C—C bond cleavage of oxygenated hydrocarbons and reforming, which results in the formation of significant amounts of CO_2 and H_2 [9,10,30].

3.2.2. *Glycerol HDO at moderate H_2 pressure*

When 0.7 MPa of H_2 were present in the reactor, glycerol HDO increased in all cases because the hydrogenation step was facilitated. The results for the Na-free catalysts are shown in Fig. 10. The bimetallic CuPd catalysts had the highest activity per gram of catalyst. They had a synergic increase in activity caused by the formation of the CuPd alloy nanoparticles. In contrast, when a physical mixture of the monometallic catalysts was used, the conversion of glycerol was practically the sum of the conversions with the monometallic, i.e. each metal acted independently during reaction. To further compare the catalytic activity of our materials we estimated the initial glycerol turnover frequency (TOF) using the reaction data for the first hours of operation, together with the metallic dispersions reported in Table 3. As Table 7 shows for Na-free catalysts, CuPdT had the largest TOF, whereas TOF with PdT, CuT and their physical mixtures were similar.

The product selectivities after 6 h of reaction using Na-free mono- and bimetallic catalysts are also reported in Table 7. The highest selectivities to 1,2-PDO (between 75 and 77%) were achieved with the CuT and CuPdT catalysts, whereas the lowest 1,2-PDO selectivity (around 14.1%) was obtained with PdT. In the case of the CuT catalyst, the major product identified in the liquid phase was 1,2-PDO, together with a smaller amount of acetol and minor amounts of alcohols (ethanol, methanol and *n*-propanol); gas phase products were not important. PdT was much less selective to 1,2-PDO and acetol because C—C scission and secondary HDO occurred significantly and led to the formation of alcohols in minor amounts (ethanol, methanol and *n*-propanol) as well as traces of acetaldehyde, propanal, acetone, acetic acid and ethylene glycol. Reforming became important, the selectivity to CO and CO_2 was ~8.4%.

When TiO_2 was modified with NaOH, the activity of all of our catalysts was enhanced. That was reflected in the conversion of glycerol at a given time, and in the initial glycerol TOF, reported in Fig. 11 and Table 8. The Cu-Pd bimetallic catalysts were again the most active, and they were also the most selective. When the fresh bimetallic (CuPdT-Na-F) was used, the glycerol conversion after 6 h of reaction reached 65% compared with 39% without Na, and the selectivity to 1,2-PDO reached 85%. The initial TOF values were also the highest with this catalyst.

Table 7
Glycerol conversion, carbon selectivity and carbon balance for Na-free catalysts with external addition of hydrogen.

Catalyst	Glycerol conversión (%)	Carbon selectivity (%)					TOF Glycerol/10^{-2} (s^{-1})	Carbon balance (%)
		1,2-PDO	Acetol	CO_2	CO	Other*		
CuT	13.0	78.3	20.7	0.2	0	0.8	4.2	98
CuT-R1	5.3	84.0	14.0	2.0	0	0	2.9	99
PdT	16.0	14.1	47.9	7.5	0.9	29.6[a]	5.5	97
CuT + PdT	26.3	63.9	12.4	8.4	1.3	14.0	3.6[b]	96
CuPdT	39.2	75.6	21.8	0.8	0	1.8	6.0[b]	98

Reaction conditions: 20 wt% glycerol aqueous solution (50 mL), 0.7 MPa H_2 pressure, 0.3 g catalyst, 220 °C, 6 h. * Other products include minor amounts of alcohols (ethanol, methanol (selectivity <2%) and *n*-propanol), as well as traces of oxygenates such as acetaldehyde, propionaldehyde, acetone, ethylene glycol (selectivity <4%), acetic acid and propionic acid, which were identified by mass spectrometry. [a] For PdT catalyst the others include majorly ethylene glycol (selectivity ~23%). [b] TON based on surface Cu + Pd sites.

Table 8
Glycerol conversion, carbon selectivity and carbon balance for Na promoted catalysts with external addition of hydrogen.

Catalyst	Glycerol conversion (%)	Carbon selectivity (%)					TOF Glycerol/10^{-2} (s^{-1})	Carbon balance (%)
		1,2-PDO	Acetol	CO_2	CO	Other*		
CuT-Na	16.0	68.0	30.1	0.3	0	1.6	9.0	97
PdT-Na	21.7	17.4	30.4	9.8	0.7	41.7[a]	8.7	94
CuT-Na + PdT-Na	34.3	52.2	11.2	9.1	0.5	27.0	5.2[b]	97
CuPdT-Na-F	65.0	85.1	8.3	1.4	0.1	5.1	14.3[b]	94
CuPdT-Na-R1	56.8	76.3	9.6	1.4	0	12.7	8.9[b]	97
CuPdT-Na-R2	56.1	81.0	7.4	1.7	0	9.9	9.7[b]	97
CuPdT-Na-R3	55.8	80.4	7.0	1.4	0	11.2	10.1[b]	98
CuPdT-Na-R4	56.9	75.6	10.5	1.6	0	12.3	9.6[b]	98
CuPdT-Na-W	55.8	89.0	6.8	0.6	0	3.6	10.8[b]	94
CuPdT-0.5Na	58.5	92.4	7.1	0.5	0	0	9.1[b]	95
CuPdT-0.5Na-R1	59.6	93.0	6.4	0.6	0	0	9.3[b]	96

Reaction conditions: 20 wt% glycerol aqueous solution (50 mL), 0.7 MPa H_2 pressure, 0.3 g catalyst, 220 °C, 6 h. * Other products include minor amounts of alcohols (ethanol, methanol (selectivity <2%) and *n*-propanol), as well as traces of oxygenates such as acetaldehyde, propionaldehyde, acetone, ethylene glycol (selectivity <3%), acetic acid and propionic acid, which were identified by mass spectrometry. [a] For PdT-Na catalyst the others include majorly ethylene glycol (selectivity up to 33%). [b] TON based on surface Cu + Pd sites.

Table 9
Glycerol hydrodeoxygenation over Cu-based mono- and bimetallic catalysts – Comparison with reports in the literature.

P_{H2} (MPa)	T (°C)	Time (h)	Catalyst	Glycerol/Catalyst ratio	$X_{Glycerol}$ (%)	$S_{1,2\text{-PDO}}$ (%)	$Y_{1,2\text{-PDO}}$ (%)	TON Glycerol/10^2	Ref.
7.0	220	12	Nanostructured Cu (Cu:Al)	125.0	47.0	88.0	41.4	0.4	[5]
2.0	200	10	$Pd_{0.04}Cu_{0.4}/Mg_{5.56}Al_2O_{8.56}$	8.0	95.0	96.1	91.3	1.2	[15]
6.4	180	12	Cu/SiO_2 + 0.54 wt.% Na	20.0	27.2	98.5	26.8	0.6	[30]
3.0	220	20	$Cu_{0.4}Mg_{5.6}Al_2(OH)_{16}CO_3$	8.0	99.1	97.0	96.1	16.9	[51]
4.0	200	12	Cu/Bohemite	20.0	77.5	92.5	71.7	1.2	[52]
9.0	180	12	Cu/SiO_2	20.0	35.0	93.7	32.8	1.1	[53]
6.0	200	6	Cu-ZnO-Al_2O_3	N.R	31.8	90.1	28.7	0.3	[54]
4.0	200	24	Cu/hectorites	20.0	50.2	76.0	38.2	1.0	[55]
6.4	200	12	Cu/SiO_2	20	73.4	94.3	69.2	2.1	[56]
0.7	220	6	Cu-Pd/TiO_2-Na	34.0	65.0	85.0	55.3	18.5	T.W.

We could not readily compare TOF values for our catalysts with results in the literature because of the lack of conversion-time data or of catalyst characterization. However, we selected reports which included Cu dispersion and calculated their glycerol turnover number (TON), an estimation of the integrated activity of the catalysts in an experimental run. As Table 9 shows, our CuPdT-Na catalyst had the highest TON (~18.5×10^2), in some cases an order of magnitude higher than most other Cu-based mono- and bimetallic catalysts under reaction conditions similar to ours [5,15,30,51–56]. This was accomplished with a reusable catalyst (see next section) in less time and at a much lower H_2 pressure.

3.2.3. Stability of the catalysts

In order to determine the stability of our catalysts we ran different tests with some of them. They included catalyst reuse after simple filtering and water rinsing, lixiviation with water prior to reaction, and a ten-fold decrease in Na content during synthesis. When we reused the CuT catalyst, there was a significant decrease in conversion and TOF (reported in Table 7). The glycerol conversion after 6 h of reaction decreased from 13.0% to 5.3%, and the initial TOF decreased from 4.2×10^{-2} to 2.9×10^{-2} s^{-1}. XRD characterization after reaction showed that CuO and Cu_2O were present, and that the Cu^0 diffraction peaks were narrower. About 14.3% of Cu leached to the reaction solution (Table 10), and the Cu dispersion (corrected for the Cu loss) decreased from 15.5% in the fresh catalyst to 10.5% after reaction. These results suggest that the underlying deactivation mechanism involves the dissolution/oxidation of some of the smaller Cu nanoparticles, rather than sintering, the common explanation in the literature [15,57]. In contrast with the changes suffered by Cu catalysts, Pd leaching or oxidation was not detected in any of the samples studied.

When the bimetallic CuPdT-Na catalyst was reused once, the activity decreased slightly, see Table 8, and it then remained approximately constant during further reuses. The selectivity to acetol and 1,2-PDO also decreased marginally during the first reuse and then stabilized. The bimetallic catalysts did not exhibit Cu or Pd leaching during reaction (see Table 10), because of the formation of stable CuPd alloy nanoparticles. There was also a stabilizing

Table 10
Cu, Pd and Na content for fresh and used mono- and bimetallic catalysts.

Catalyst	Na load wt%		Na leaching%	Cu load wt%		Cu leaching%
	Fresh	Used		Fresh	Used	
CuT	0	0	0	4.7	4.0	14.3
CuT-Na	4.9	1.1	77.6	4.9	4.5	8.2
PdT	0	0	0	0	0	0
PdT-Na	4.8	0.9	81	0	0	0
CuPdT	0	0	0	4.9	4.7	4.1
CuPdT-Na-F	4.8	1.0	79.2	4.8	4.8	0
CuPdT-Na-W	1.6	0.4	75	4.8	4.8	0
CuPdT-Na-R1	1.0	0.5	50	4.8	4.8	0
CuPdT-Na-R2	0.5	0.5	0	4.8	4.8	0
CuPdT-Na-R3	0.5	0.5	0	4.8	4.8	0
CuPdT-0.5Na	0.41	0.40	2.4	4.7	4.7	0
CuPdT-0.5Na-R1	0.40	0.39	2.5	4.7	4.7	0

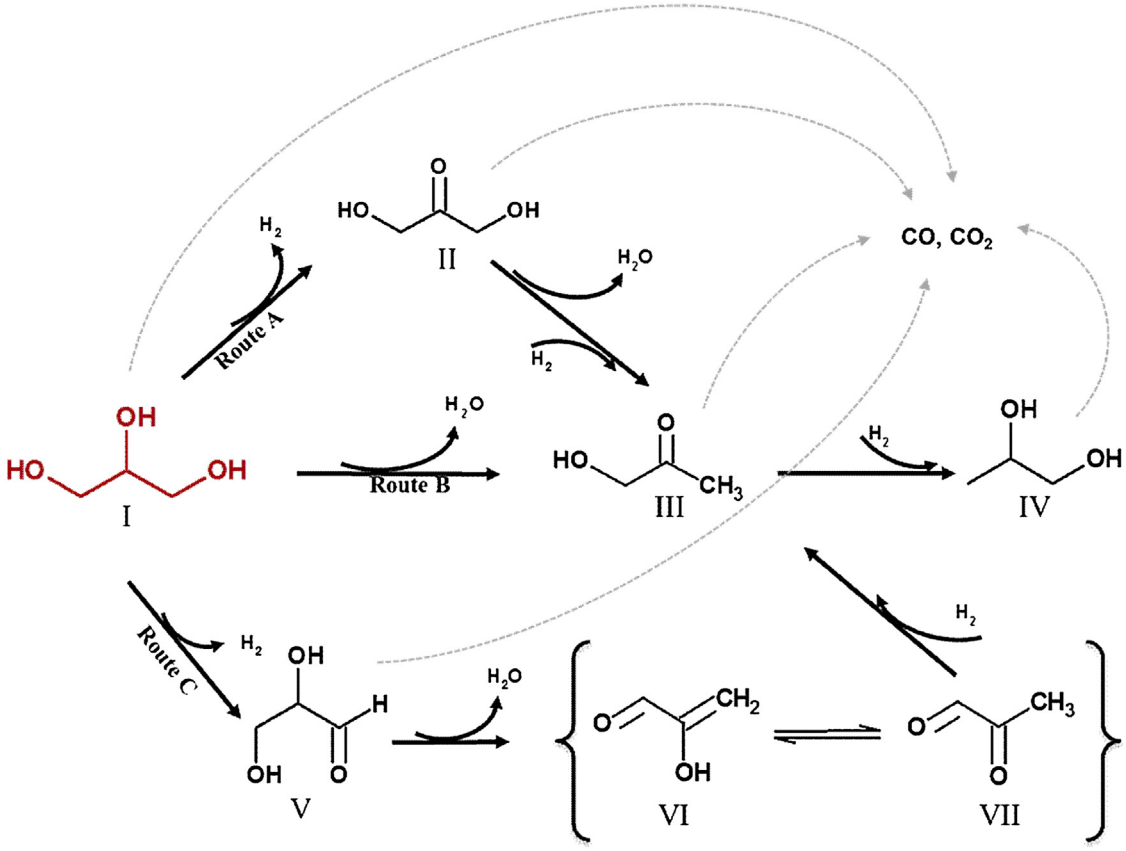

Fig. 12. Reaction pathways for the formation of 1,2-PDO from glycerol by acetol routes under alkaline conditions. I: Glycerol, II: Di-hydroxyacetone, III: Acetol, IV: 1,2-PDO, V: Glyceraldehyde, VI: 2-Hydroxyacrolein, VII: Pyruvaldehyde.

effect of Cu when Na was added to the support, as mentioned in the literature [15,57].

The variation in reactivity during the first reuse appears to be caused by the initial loss of Na from the fresh catalyst to the reaction solution, as well as the formation of Na_2CO_3 on the catalyst. AAS analysis of the reaction media showed that close to 80% of the Na initially present in the mono- and bimetallic catalysts was found in solution after the first use (Table 10). Leaching of Na decreased during further uses until Na in the catalyst reached a stable residual level (0.5 wt%). That content was enough to sustain significant conversion and selectivity towards 1,2-PDO in levels similar to those attained with a freshly synthesized catalyst with low-Na (CuPdT-0.5Na). Cleavage of the C—C bonds, catalyzed by NaOH in the liquid phase [9,10,30,51], was not important when the Na-bearing solid catalysts were used, probably because the concentration of Na in solution was small and the pH of the reaction solution decreased as the reaction proceeded. The initial pH (pHo) of the reaction medium in the presence of the catalysts with Na was about 10.5, whereas pHo of the solution in contact with the catalysts without Na was 5.5. The fact that we the catalysts were reused by simple washing and filtering is further proof that the reaction occurs on the surface of the catalyst and that it is not catalyzed by dissolved metal cations.

3.2.4. *Catalyst structure, activity and selectivity*

Perhaps the most important structural feature that makes Cu-Pd systems singular during the catalytic hydroconversion of glycerol with bimetallic Cu-Pd/TiO_2-Na material is the presence of stable

CuPd alloy nanoparticles formed during synthesis and with diameters close to 4.0 nm. Another aspect that merits attention is the surface enrichment of the nanoparticles with Cu, which favors the HDO pathway, a characteristic of Cu. The combination of those two factors results in an active catalysts because of the small nanoparticle diameters, highly selective to HDO because of their Cu-like surface.

Although the mechanism of the hydroconversion of glycerol catalyzed by supported metals is complex, as evidenced by the studies reported in the literature [7,20,21], our bimetallic catalysts are very selective to HDO and they presumably activate a reaction pathway to 1,2-PDO that proceeds through acetol, or an intermediate closely related to this compound. Of the different routes leading to acetol from glycerol, given in Fig. 12, under aqueous conditions glycerol reacts primarily via route B, i.e. through dehydration catalyzed by sites on the oxidic support [50]. Acetol readily converts to 1,2-PDO by hydrogenation primarily on the Cu metal sites. The enhancement caused by the presence of Na on the support appears to stem from the formation of basic sites that favor dehydration, not by the activation of a parallel homogeneous reaction.

The HDO activity of Cu sites in the bimetallic catalysts increases presumably as a result of the activation/generation of H_2 on Pd sites located on the same nanoparticle. Such coupling helps explain why there is very good activity at a H_2 pressure much below the values normally used. Our structural results also help explain reports about the activation of HDO by Pd-Cu in the absence of H_2 [19], an effect apparently not observed with other bimetallic systems [57].

4. Conclusions

We have developed a Cu-Pd bimetallic catalyst supported on TiO_2-Na that is active, selective and stable during glycerol hydrodeoxygenation towards 1,2-PDO at 0.7 MPa H_2, a pressure significantly lower than in most reports on the subject.

The high activity and selectivity towards 1,2-PDO of the Cu-Pd bimetallic catalysts was ascribed to the formation of stable CuPd alloy nanoparticles formed during low-temperature reduction, as evidenced by XRD, H_2-TPR, chemisorption-titration, HRTEM, and SAED. They have an average diameter well below the diameter of Cu or Pd monometallics. Formation of this alloy stabilizes Cu^0 against leaching and oxidation, and results in a reusable catalyst.

Pd sites on the surface of the nanoparticles favor the generation of H_2 *in situ* from glycerol reforming and, in general, the activation of H_2. Thus, with Cu-Pd/TiO_2-Na we can use low H_2 pressures during the selective production of 1,2-PDO from glycerol.

Na reaches a stable value (0.5 wt.%) on TiO_2 upon reuse and that is enough to have a positive effect upon both the conversion of glycerol and the selectivity towards 1,2-PDO. The presence of Na also helps prevent the leaching of Cu in monometallic catalysts.

Acknowledgments

This research was made possible by the financial support of Universidad A. Metropolitana-Iztapalapa, México. A.N. Ardila acknowledges Politécnico Colombiano Isaza, Enlaza Mundos (Colombia) and CONACYT (Mexico) for a graduate fellowship. ALV acknowledges financial support from Universidad de Antioquia.

Appendix A. Supplementary data

Supplementary data associated with this article can be found, in the online version, at http://dx.doi.org/10.1016/j.apcatb.2017.08.006.

References

[1] D. Roy, B. Subramaniam, R.V. Chaudhari, Catal. Today 156 (2010) 31–37.
[2] Z. Yuan, J. Wang, L. Wang, W. Xie, P. Chen, Z. Hou, X. Zheng, Bioresour. Technol. 101 (2010) 7088–7092.
[3] M. Balaraju, K. Jagadeeswaraiah, P.S. Sai Prasad, N. Lingaiah, Catal. Sci. Technol. 2 (2012) 1967–1976.
[4] L.C. Meher, R. Gopinath, S.N. Naik, A.K. Dalai, Ind. Eng. Chem. Res. 48 (2009) 1840–1846.
[5] R.B. Mane, A.M. Hegne, A.A. Ghalwadkar, S. Vijayanand, P.H. Mohite, H.S. Potdar, S.V. Rode, Catal. Lett. 135 (2010) 141–147.
[6] Z. Yuan, P. Wu, J. Gao, X. Lu, Z. Hou, X. Zheng, Catal. Lett. 130 (2009) 261–265.
[7] O.M. Daniel, A. DeLaRiva, E.L. Kunkes, A.K. Datye, J.A. Dumesic, R.J. Davis, ChemCatChem 2 (2010) 1107–1114.
[8] Y. Shinmi, Y. Koso, S. Kubotac, T. Nakagawa, Y. Tomishige, Appl. Catal. B 105 (2011) 117–127.
[9] E.P. Maris, R.J. Davis, J. Catal. 249 (2007) 328–337.
[10] E.P. Maris, W.C. Ketchie, M. Murayama, R.J. Davis, J. Catal. 251 (2007) 281–294.
[11] E.S. Vasiliadou, T.M. Eggenhuisen, P. Munnikc, P.E. de Jongh, K.P. de Jong, A.A. Lemonidou, App. Catal. B: Environ. 145 (2014) 108–119.
[12] S. Wang, H. Liu, Catal. Lett. 117 (2007) 62–67.
[13] A. Bienholz, F. Schwab, P. Claus, Green Chem. 12 (2010) 290–295.
[14] A. Bienholz, R. Blume, A. Knop-Gericke, F. Girgsdies, M. Behrens, P. Claus, J. Phys. Chem. C 115 (2011) 999–1005.
[15] S. Xia, Z. Yuan, L. Wang, P. Chen, Z. Hou, App. Catal. A: Gen. 403 (2011) 173–182.
[16] X. Shuixin, Z. Liping, N. Renfeng, C. Ping, L. Hui, H. Zhaoyin, Chin. J. Catal. 34 (2013) 986–992.
[17] S. Xia, Z. Yuan, L. Wang, P. Chen, Z. Hou, Bioresour. Technol. 104 (2012) 814–817.
[18] I. Gandarias, S.G. Fernández, M. El Doukkali, J. Requies, P.L. Arias, Top. Catal. 56 (2013) 995–1007.
[19] X. Jin, L. Dang, J. Lohrman, B. Subramaniam, S. Ren, R.V. Chaudhar, ACS Nano 7–2 (2013) 1309–1316.
[20] G.W. Huber, J.W. Shabaker, S.T. Evans, J.A. Dumesic, Appl. Catal. B: Environ. 62 (2006) 226–235.
[21] R.R. Davda, J.W. Shabaker, G.W. Huber, R.D. Cortright1, J.A. Dumesic, App. Catal. B: Environ. 56 (2005) 171–186.
[22] J. Duan, Y.T. Kim, H. Lou, G.W. Huber, Catal. Today 234 (2014) 66–74.
[23] R.M. Ravenelle, J.R. Copeland, A.H. Van Pelt, J.C. Crittenden, C. Sievers, Top. Catal. 55 (2012) 162–174.
[24] D.C. Elliott, T.R. Hart, G.G. Neuenschwander, Ind. Eng. Chem. Res. 45 (2006) 3776–3781.
[25] A.J. Renouprez, K. Lebas, G. Bergeret, J. Mol. Catal. A 120 (1997) 217–225.
[26] M.H. Kim, J.R. Ebner, R.M. Friedman, M.A. Vannice, J. Catal. 208 (2002) 381–392.
[27] L.S. Vadlamannati, V.I. Kovalchuk, J.L. d'Itri, Catal. Lett. 58 (1999) 173–178.
[28] A. Gervasini, S. Bennici, Appl. Catal. A 281 (2005) 199–205.
[29] Y. Ma, T. Matsushima, Catal. Today 111 (3–4) (2005) 302–306.
[30] Z. Huang, F. Cui, H. Kang, J. Chen, C. Xia, App. Catal. A: Gen. 366 (2009) 288–298.
[31] R.B. Manea, S.E. Kondawar, P.S. Niphadkar, P.N. Joshi, K.R. Patil, C.V. Rode, Catal. Today 198 (2012) 321–329.
[32] J. Batista, A. Pintar, D. Mandrino, M. Jenko, V. Martin, Appl. Catal. A: Gen. 206 (2001) 113–124.
[33] A. Edelmanna, W. Schießer, H. Vinek, A. Jentys, Catal. Lett. 69 (2000) 11–16.
[34] J. Sá, S. Gross, H. Vinek, App. Catal. A: Gen. 294 (2005) 226–234.
[35] S.K. Kim, J.H. Lee, I.Y. Ahn, W.-J. Kim, S.H. Moon, App. Catal. A: Gen. 401 (2011) 12–19.
[36] P. Panagiotopoulou, D.I. Kondarides, J. Catal. 267 (2009) 57–66.
[37] Z. Wu, Z. Sheng, H. Wang, Y. Liu, Chemosphere 77 (2009) 264–268.
[38] X. Zhu, M. Shen, L.L. Lobban, R.G. Mallinson, J. Catal. 278 (2011) 123–132.
[39] G. Colón, M. Maicu, M.C. Hidalgo, J.A. Navío, App. Catal. B: Environ. 67 (2006) 41–51.
[40] I. Witonska, A. Królak, S. Karski, J. Mol. Catal. A: Chem. 331 (2010) 21–28.
[41] A. Gaspar, I. Dieguez, App. Catal. A: Gen. 201 (2000) 241–251.
[42] N. Babu, R. Lingaiah, P. Gopinath, P. Reddy, P.S. Prasad, J. Phys. Chem. C 111 (2007) 6447–6453.
[43] H. Lieske, J. Vólter, J. Phys. Chem. 89 (1985) 1–2.
[44] E.B. Fox, S. Velu, M.H. Engelhard, Y.H. Chin, J.T. Miller, J. Kropf, C. Song, J. Catal. 260 (2008) 358–370.
[45] A.M. Molenbroek, S. Haukka, B.S. Clausen, J. Phys. Chem. B 102 (1998) 10680–10689.
[46] J.M. Moreno, M.A. Aramendía, J.M. Marinas, F.J. Urbano, Appl. Catal. B: Environ. 76 (2007) 34–41.
[47] K. Sun, J. Liu, N.K. Nag, N.D. Browning, J. Phys. Chem. B 106 (2002) 12239–12246.
[48] M. Fernández-García, J.A. Anderson, G.L. Haller, Phys. Chem. 100 (1996) 16247–16254.
[49] B. Heinrichs, F. Noville, J.-P. Schoebrechts, J.-P. Pirard, J. Catal. 192 (2000) 108–118.
[50] B. Peng, C. Zhao, I. Mejía-Centeno, G.A. Fuentes, A. Jentys, J.A. Lercher, Catal. Today 183 (2012) 3–9.
[51] Z. Yuan, L. Wang, J. Wang, S. Xia, P. Chen, Z. Hou, X. Zheng, App. Catal. B: Environ. 101 (2011) 431–440.

[52] Z. Wu, Y. Mao, M. Song, X. Yin, M. Zhang, Catal. Commun. 32 (2013) 52–57.
[53] Z. Huanga, F. Cui, J. Xue, J. Zuo, J. Chen, C. Xia Catal, Today 183 (2012) 42–51.
[54] S. Wang, H. Liu, Chin. J. Catal. 35 (2014) 631–643.
[55] T. Sánchez, P. Salagre, Y. Cesteros, A. Bueno-López, Chem. Eng. J. 179 (2012) 302–311.
[56] Z. Huang, F. Cui, H. Kang, J. Chen, X. Zhang, C. Xia, Chem. Mater. 20 (2008) 5090–5099.
[57] J. Chaminand, L. Djakovitch, P. Gallezot, P. Marion, C. Pinel, C. Rosier, Green Chem. 6 (2004) 359–361.